Accounting for the effect of dislocation climb-mediated flow on the anisotropy and texture evolution of Mg alloy, AZ31B

Ritzo, Michael
Lebensohn, Ricardo A.
Capolungo, Laurent
Agnew, Sean

To be published in: Materials Science and Engineering: A

DOI to publisher's version: 10.1016/j.msea.2021.142581

Permalink to record: http://permalink.lanl.gov/object/view?what=info:lanl-repo/lareport/LA-UR-21-32403

Journal Pre-proof

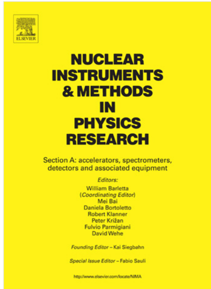

Comparison of MCNP thermal scattering laws to inelastic neutron scattering data

C.M. Lavelle, K.K.H. Leung, T.M. Ito

PII: S0168-9002(21)01092-5
DOI: https://doi.org/10.1016/j.nima.2021.166255
Reference: NIMA 166255

To appear in: *Nuclear Inst. and Methods in Physics Research, A*

Received date : 9 February 2021
Revised date : 13 December 2021
Accepted date : 18 December 2021

Please cite this article as: C.M. Lavelle, K.K.H. Leung and T.M. Ito, Comparison of MCNP thermal scattering laws to inelastic neutron scattering data, *Nuclear Inst. and Methods in Physics Research, A* (2021), doi: https://doi.org/10.1016/j.nima.2021.166255.

Comparison of MCNP Thermal Scattering Laws to Inelastic Neutron Scattering Data

C. M. Lavelle[a,*], K. K. H. Leung[b,c], T. M. Ito[d]

[a] The Johns Hopkins University Applied Physcs Laboratory, 11100 Johns Hopkins Road, Laurel, MD, 21784, USA
[b] Montclair State University, 1 Normal Ave, Montclair, NJ 07043, USA
[c] Triangle Universities Nuclear Laboratory, 116 Science Drive, Durham, North Carolina 27708, USA
[d] Los Alamos National Laboratory, Los Alamos, New Mexico 87545, USA

Abstract

Neutron transport computations employ thermal scattering laws (TSLs) to account for the influence of material structure and collective excitations at low energy ($\lesssim$ 10 eV). Recent work has been undertaken to improve TSL accuracy and expand the number of available materials in the Evaluated Nuclear Data File (ENDF). However, comparison of TSL to measured data is often sparse. We present a method to evaluate TSL accuracy in the Monte Carlo N-Particle (MCNP) code by simulating inelastic neutron scattering (INS) measurement and comparing to data. The method is briefly described with example application to the recently released ENDF-VIII TSL library for polyethylene as well as a cryogenic PE TSL we are separately developing.

Keywords: Thermal neutron, Scattering Law, TSL, ultra-cold neutron, neutron, electric dipole moment

1. Introduction

Neutron transport simulation requires accurate data in order to achieve accurate results. Low energy neutron interaction ($\lesssim$ 10 eV) is strongly affected by the atomic structure and collective excitations of the medium. [1] A modification to nuclear scattering by the dynamic structure factor, $S(Q, \omega)$, accounts for these effects.

The implementation of $S(Q, \omega)$ in the context of neutron transport is referred to as a thermal scattering law (TSL). [2, 3, 4] The Monte Carlo N-Particle (MCNP) radiation transport code [5] is a tool of choice for transport computation, but the library of materials with a TSL is limited. Recent work improved upon earlier TSLs [6] and expanded the list of available materials for the Evaluated Nuclear Data File (ENDF) VIII release. [7]

A number of experimental and computational techniques have applied to TSL development, including inelastic neutron scattering (INS) measurement [8, 9, 10], total cross-section measurement [11], and condensed matter modeling techniques. [7, 12, 13] ENDF-VIII's TSL library benefits from these efforts.

Modern INS measurements provide a rich data source for evaluating TSLs. [6, 7, 12] In this paper we suggest a simple means to compare TSLs and INS data. The intent is to provide global test of the TSL, including the probability tables derived from the condensed matter physics and its sampling, here specialized to the MCNP code. The method is demonstrated using polyethylene (PE) TSLs from the ENDF VII.I and ENDF-VIII libraries [7] and a 5 K PE model we have separately developed. An earlier measurement campaign provides the INS dataset. [8] We expect the method to be of interest to workers engaged in TSL development and evaluation.

2. Incoherent Inelastic Neutron Scattering

The dynamic structure factor is related to the double differential scattering cross-section as

$$\frac{d^2\sigma}{d\Omega dE} = \frac{\sigma_b}{4\pi}\frac{k'}{k}S(Q, \omega) \quad (1)$$

*corresponding author: chris.lavelle@jhuapl.edu

where σ_b is the bound atom cross-section and k and k' are the initial and final state wave vector, respectively.

TSLs within MCNP use the incoherent approximation for isotropic media. All dynamics are considered incoherently, and elastic scattering is assumed to be entirely incoherent for a strong incoherent scattering atom such as H. The parameters are energy transfer, $\hbar\omega$,

$$\hbar\omega = E - E' \tag{2}$$

and wave vector transfer, Q,

$$Q = |\vec{k'} - \vec{k}| \tag{3}$$

where E and E' are the initial and final state energies respectively. Energy and momentum transfer, $\hbar Q$, are related to each other by cosine of the scattering angle, μ, as

$$\frac{\hbar^2 Q^2}{2m} = E' + E - 2\mu\sqrt{EE'} \tag{4}$$

where m is the neutron mass.

2.1. TSL Preparation with NJOY

MCNP TSLs are usually created by the NJOY code, a series of modules run sequentially to generate formatted data for MCNP. [14] Briefly, the process is as follows.

The LEAPR module uses a series of user input parameters such as the generalized density of states (GDOS), temperature, and scattering length to calculate a dimensionless version of $S(Q,\omega)$. [15] In this work, we rely on incoherent scattering only. However, the LEAPR module is flexible, and can also create TSLs to represent the scattering from diffusion in liquids, the relative motions in gases, coherent elastic scattering (diffraction) in solids, and ortho- and para- hydrogen and deuterium spin-dependent interactions.

A second module, THERMR, prepares an energy-angle probability table based the results of the LEAPR module. Finally, the ACER module prepares this table in an MCNP compatible format.

2.2. INS Measurement

Measurements were carried out at the Spallation Neutron Source (SNS) Wide Angle Chopper Spectrometer (ARCS) instrument. [16] ARCS employs a chopper system to create a mono-energetic neutron beam from a pulsed, water moderated neutron source. Final state energy information is determined from time of flight (ToF) and the scattering angle is registered by cylindrical array of position sensitive detectors subtending a wide solid angle. A single scatter in the material is assumed, and a multiple scattering correction may be required for thick samples. [17]

This measurement technique can be analogously created within MCNP using a simple tally. The source is a monoenergetic neutron beam of zero extent (pencil beam) directly incident on a small spherical sample. A particle current tally across a spherical surface centered on the sample, illustrated in Fig. 1, "measures" the inelastic neutron scattering predicted by the TSL. The tally is the integrated particle current, $\Phi(E,\mu)$, over a discrete region of phase space, ΔE and $\Delta\mu$. These terms are related to $S(Q,\omega)$ as,

$$S(Q,\omega) \propto \sqrt{\frac{1}{E'}} \frac{\Phi(E,\mu)}{\Delta\mu\Delta E} \tag{5}$$

The method requires the TSL to be prepared in the continuous format as described in Ref. [18]. Previous TSLs only scatter into discrete secondary energies and angles. [19] In that sense, this work is enabled by the advancements in INS, MCNP sampling methods, and the recent TSL development.

The tally shown in Fig. 1 is an F1-type current tally where the beam direction as the reference vector for cosine determination. A fixed reference vector for cosine determination is the FRV special tally option in the syntax of MCNP. The simulated sample is small (thickness $\ll$ 1 mean free path) to ensure the single scattering limit.

The simulation is run to high numerical precision with 1000 energy bins and 100 cosine bins. The value of the tally at each (E,μ) point's corresponding (Q,ω) coordinate is then interpolated onto the measurement's (Q,ω) coordinates for comparison. The INS measurements are not on an absolute scale and the H cross-section is dominated by incoherent scattering (80 b) compared to coherent scattering (1.8 b). Simulation and measurement are therefore normalized by the sum rule assuming purely incoherent scattering,

$$\int_{-\infty}^{\infty} S(Q,\omega) d\omega = 1. \tag{6}$$

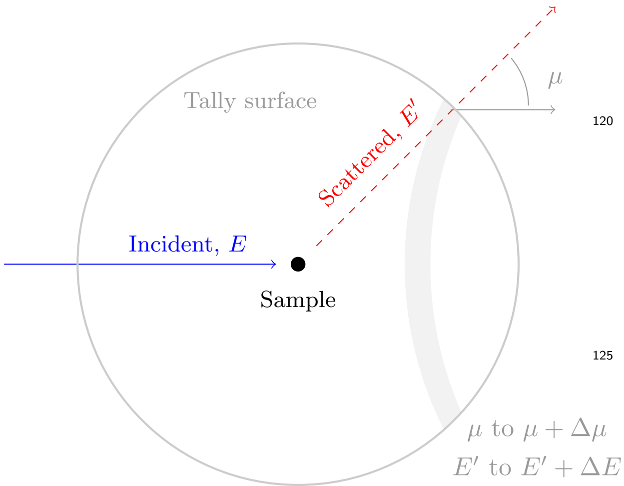

Figure 1: Inelastic neutron scattering simulation tally geometry. An incident neutron of energy E strikes the sample and scatters to energy E'. The scattered neutron's energy is recorded as it crosses the spherical tally surface. Energy is recorded in histogram bins from E' to $E' + \Delta E'$. Cosine binning of the scattering angle relative to the beam direction is recorded in bins from μ to $\mu + \Delta\mu$, as indicated by the gray band.

3. Measurements

3.1. Data Collection and Assessment

We demonstrate the technique using MCNP v6.1, employing the ENDF TSLs for 294 K PE [20] and a PE TSL we have developed at 294 K and 5 K. The sample is a 10 μm thick high density PE (HDPE) film of high polymer crystallinity.

Multiple scattering corrections have not been applied to the presented measurements. These corrections are most necessary in such a thin film when the secondary neutron energy is small, such as when $\hbar\omega \sim E$. At 1 meV, for example, the HDPE total scattering cross-section gives a mean free path, λ, of 1.0 mm assuming density of 0.95 g cm^{-3}. [8] In this case, the probability to multiple scatter rises to 10% only for scattering angles into the plane of the sample, $|\mu| \lesssim 0.08$. Such in plane scattering would be somewhat attenuated by the cadmium lined sample frame. Furthermore, a multiple scattered neutron would be registered in a broad angular distribution [17], further diluting its contribution. We therefore reasonably expect single scatter to dominate.

Instrumental energy resolution broadens the $S(Q,\omega)$ measurement. This is particularly apparent for the elastic peak, which is exactly $\hbar\omega = 0$ in simulation but instrumentally broadened in measurement. The TSL can only be evaluated within this measurement resolution, despite the simulation having ideal energy resolution. Simulation results are therefore shown convoluted with energy resolution.

4. Results

4.1. ENDF PE at Ambient Temperature

4.1.1. General $S(Q,\omega)$ comparison

An example contour plot of $S(Q,\omega)$ for ambient temperature PE simulation and measurement is shown in Fig. 2. Incident neutron energy is 250 meV. Measurement temperature is uncontrolled ambient conditions, and simulation is the the ENDF-VIII model at 294 K.

4.2. Instrumental Resolution

A more qualitative assessment of agreement can be made by plotting the resolution-broadened simulation of $S(Q,\omega)$ at fixed values of Q, rather than the general contour shown in Fig. 2. The resolution function is asymmetric, as described in Ref. [16], and its width varies with both incident neutron energy and the measured momentum and energy transfers. The resolution function was computed by the instrument science team and convoluted with the MCNP simulated $S(Q,\omega)$ terms. [21] l The effect of broadening the simulation by the ARCS resolution function is shown in Figure 3 as an example. The MCNP output shows the sharp elastic peak and high resolution over spectral features, whereas the resolution broadened functions show the asymmetric elastic peak in addition to the expected broadening of the dynamical features. It should be noted that the 675 meV incident energy measurement employed protocols for the instrument which are no longer in use, such that resolution function in present application will vary from that shown here.

4.3. Detailed Comparison

Simulation and measurement at fixed Q values are shown in Fig. 4. Simulation is shown broadened by instrumental resolution. Similar values of energy and momentum transfer can result from different values of E, E', and μ, such that we include $Q_o = 5$ Å^{-1} for each incident energy. Results at increasing Q are offset by powers of 10 for clarity.

The reader may note the deviation between TSL simulation and measurement is significant in many cases. A deficiency of this comparison method is

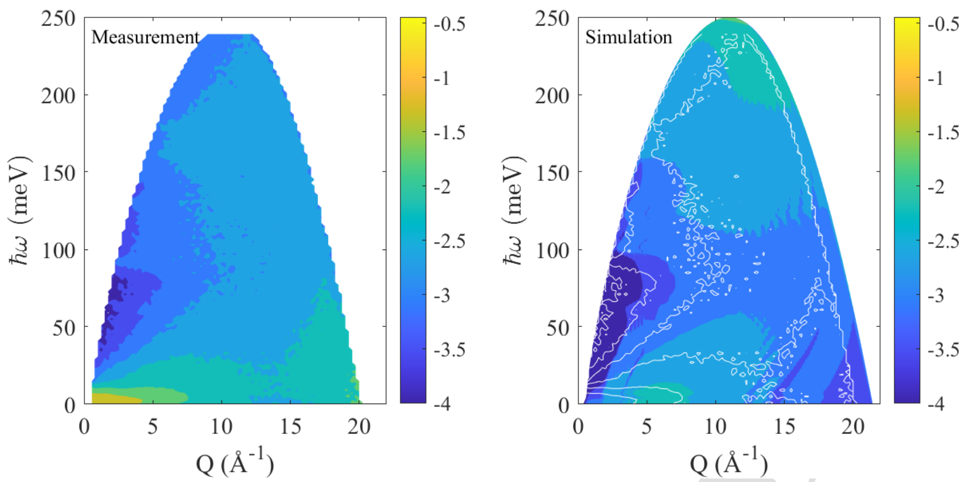

Figure 2: Comparison of ARCS measurement of 300 K HDPE at 250 meV incident neutron energy **(left)** to simulation with MCNP6.1 and the ENDF-VIII TSL **(right)**. Measurement is overlaid as the light grey lines on the simulation. Contours are $S(Q,\omega)$ in units of meV^{-1} in logarithmic powers of 10.

that it cannot tell which aspect of the TSL development is responsible for the discrepancy, be it the incoherent approximation, the NJOY code, the user's choice of inputs to NJOY, or the TSL sampling methods. For our purposes, the comparisons remain largely qualitative. However, the method provides a means for feedback between the NJOY adjustments and measured data.

We note general trends. In most cases we observe that scattering into large energy transfers (where secondary neutron energy is small) is overestimated. Secondly, scattering at small energy transfers near the elastic peak appear underestimated by the simulation. This underestimation is larger than can be attributed to instrumental resolution in the measurement. The deficiency in scattering at small energy transfer becomes more pronounced as at larger values of Q. Comparing ENDF VII.1 to ENDF VIII, we note the discrepancy is still present though at a slightly lower amount. The dispersionless excitation at $\sim$ 100 meV in measurement is shown at a slightly higher value in the $Q = 5.0$ Å^{-1} measurement 250 meV. This misplacement can be traced to the dynamics used to create the model. [20]

ENDF VIII appears to produce improved agreement compared to ENDF-VII.1, particularly at lower values of Q. Nevertheless, there are systematic differences between simulation and measurement at large energy transfer which we will see repeated in the development of our own TSL.

4.4. PE TSL under development at 294 K

A GDOS was selected from the literature [22] which closely matched the INS data at 5 K and a TSL was prepared using NJOY21. [23] This model is compared with measurement in Fig. 5.

One of the major differences between this model and ENDF is the low energy ($\hbar\omega < 70$ meV) GDOS. This deviation likely results from the ENDF-VIII model degree of crystallinity, reported in the range of 70% to 90% [24], while the model employed in our TSL development assumes 100% crystallinity. [22] The sample is 95% crystalline.

The low energy change does not appear to greatly improve agreement for 50 meV incident energy compared to ENDF-VIII for energy loss scattering ($\hbar\omega > 0$). However, slightly improved agreement for energy gain scattering is observed. Overestimation at large Q is slightly less severe in the 50 meV measurement compared to ENDF-VIII. We see similar levels of agreement elsewhere, however there is less underestimation at small energy transfer.

4.5. Cryogenic PE

We next apply the method to cryogenic PE TSL, recomputing within NJOY at 5 K. The result is compared to simulation in Fig. 6.

The cryogenic TSL shows agreement with the detailed structure of the INS result is obtained

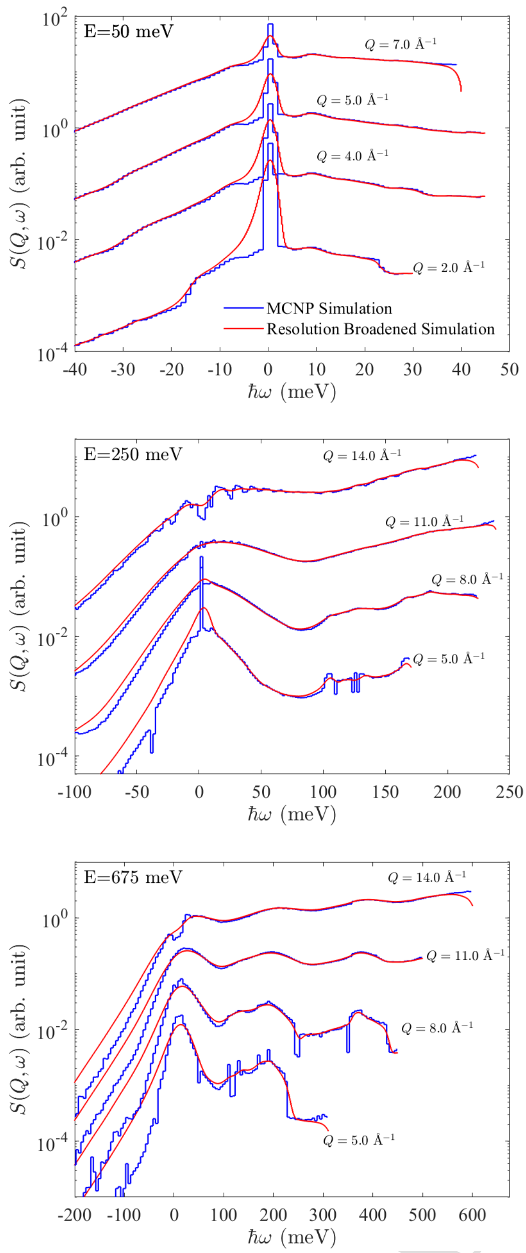

Figure 3: Comparison of simulation and simulation broadened by instrumental resolution. Note the asymmetric resolution line shape apparent at the elastic peak. The ENDF-VIII simulation model at 294 K is used.

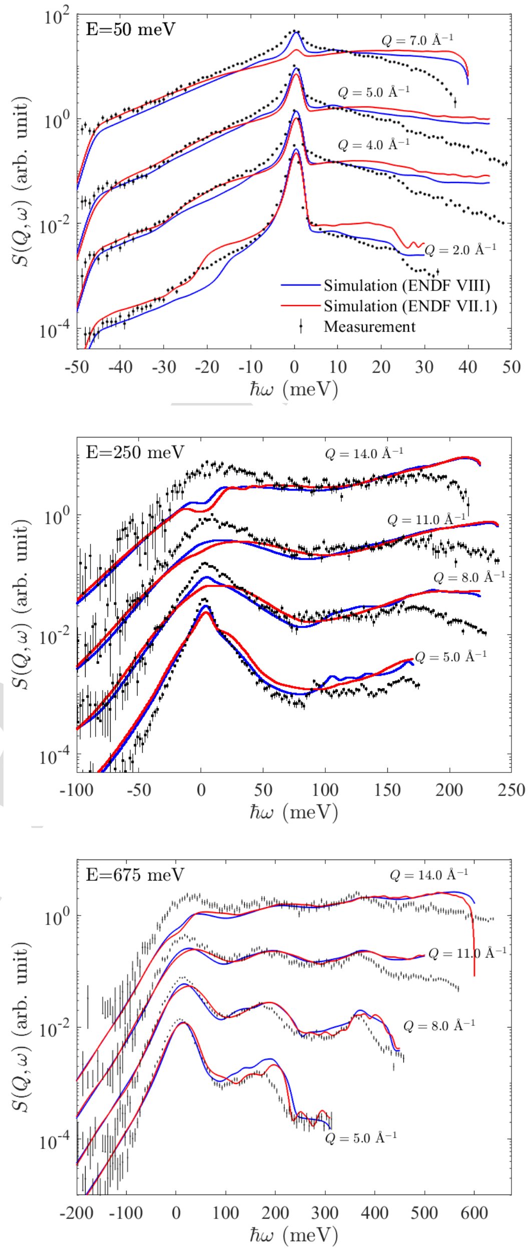

Figure 4: HDPE at 294 K compared to inelastic neutron scattering measurement at fixed $Q = Q_o$ and various incident neutron energies. Results for increasing Q_o are offset by powers of 10 for clarity. The earlier ENDF VII.1 and more recent ENDF VIII TSLs for different incident energies are shown. Simulation broadened by instrumental resolution.

for 50 meV and 250 meV incident neutron energy. Scattering at larger values of $\hbar\omega$ remains overestimated, and the quasi-elastic scattering remains underestimated. Low energy transfer behavior appears to be in good agreement for the 250 meV

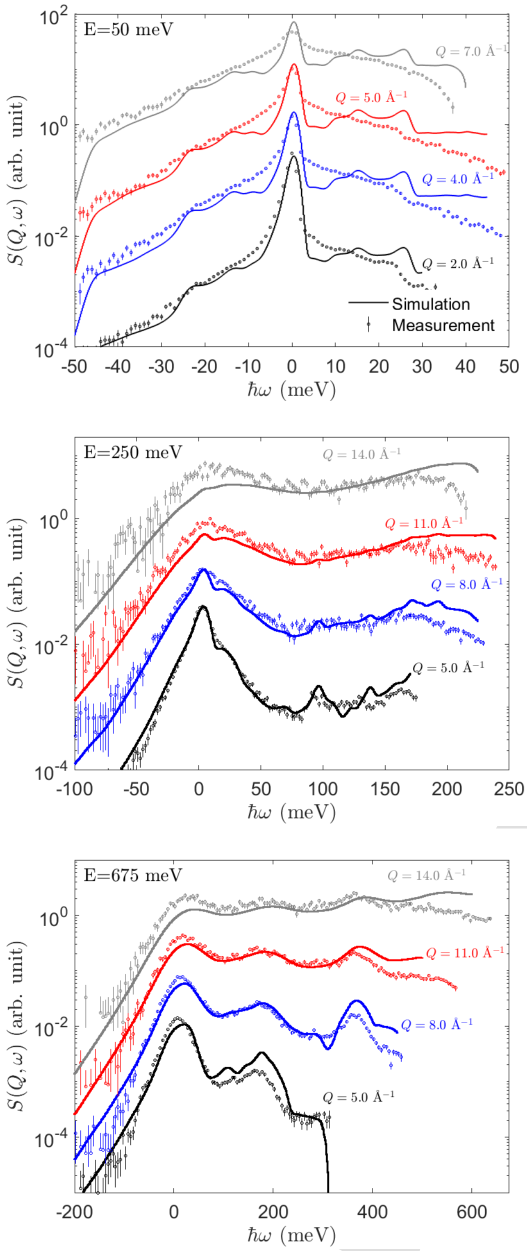

Figure 5: HDPE at 294 K using dynamics derived from literature by close comparison with measurement. [8] Results for increasing Q_o are offset by powers of 10 for clarity. Simulation broadened by instrumental resolution.

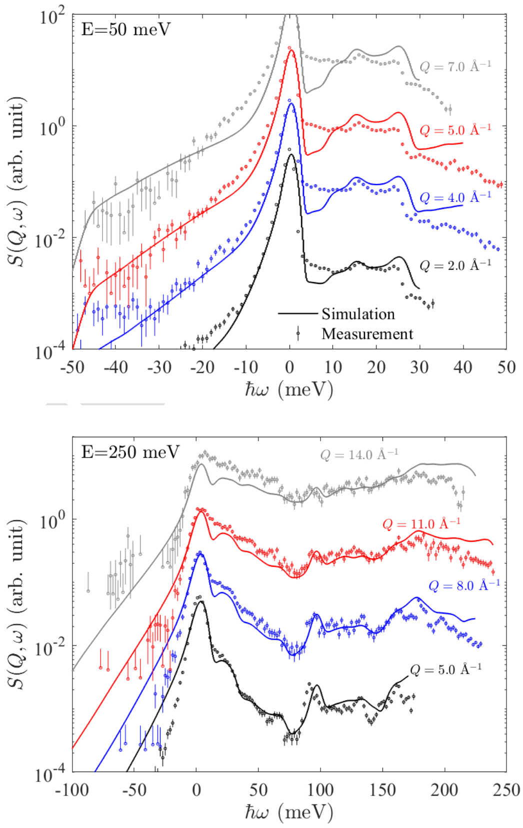

Figure 6: HDPE at 5 K using TSL model parameters tuned against scattering data. Agreement is excellent for incident energy E = 50 meV and 250 meV. Each curve is offset by 10× for clarity. Simulation is shown broadened by instrumental resolution.

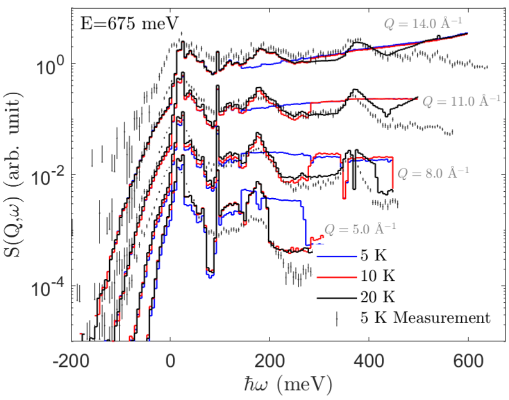

Figure 7: HDPE measurement at 5 K and $E = 675$ meV incident neutron energy compared to tuned TSL model. Agreement is satisfactory until flat regions occur at large Q. The onset energy of this region increases with temperature, disappearing entirely at 20 K. See text for discussion, the issue appears to originate within NJOY for large values of $\beta = \frac{E-E'}{k_b T}$. Each curve is offset by 10× for clarity. Simulation is not broadened by instrumental resolution.

measurement, both at very low energy transfer and the higher values of Q. The region from 100 meV to 200 meV is also closely reproduced.

The method revealed unphysical flat regions for low temperature PE at high incident energy, shown in Fig. 7. The effect appears to be related to a numerical problem within NJOY for low temperatures and presently under investigation. [12] NJOY employs dimensionless variables in its approach to the multiphonon expansion, including terms $e^{-\frac{\beta}{2}}$ where $\beta = \frac{E'-E}{k_b T}$. [15] It is noted in Ref. [15] that numerical issues may occur when β is large. In this case we see the onset of the flat region for $E = 675$ meV when $\beta \gtrsim 360$ (150 meV at 5 K and 300 meV at 10 K). It follows then that no artifacts are observed for 20 K, where $\beta = 360$ is outside the dynamic range.

5. Conclusion

A tally which can be used to compare INS data with MCNP simulation for TSL evaluation is presented. The tally recreates the $S(Q, \omega)$ as sampled by MCNP for comparison with data. We note a similar approach could be used to simulate transmission and obtain the MCNP model for total cross-section. We found this to be of less value than the dynamical analysis as the MCNP sampled model for total cross-section closely reproduced the NJOY ACER module's output. Furthermore, NJOY derived PE models have been shown elsewhere [7] to agree with ambient temperature PE total cross-section data. In that sense, the computed mean free path is acceptable in these models despite the deviations in dynamics observed in some regions.

All models for PE show underestimation of scattering in the near-elastic region as well as in the elastic region at higher incident energy and higher Q. NJOY has no means to include quasi-elastic dynamics in solids at present, enforcing a debye-like density of states at low energy, which may play a role in this deviation. Scattering into high Q at large energy transfer, essentially back-scattered neutrons with low secondary energy, is consistently over estimated in simulation.

Finally, we note that this method is a single collision benchmark and the purpose of Monte Carlo is to track particles through many collisions. We can also expect neutrons to transport through regions of phase space that may not be represented in the benchmarking measurements. It may therefore be of use to consider measuring and modeling samples of varying thickness and geometry. Comparison can be made more directly to the measurement, perhaps as a function of sample geometries which could benchmark multiple collisions. In this case, the comparison would be the time of flight scattering into each angle rather than the final state energy after processing to $S(Q, \omega)$.

Acknowledgments

We gratefully acknowledge the support of the U.S. Department of Energy Office of Nuclear Physics through Grant No. DE-AC05-00OR22725 and Contract Nos. DE-AC52-06NA25396 and 89233218CNA000001 under proposal LANLEEDM.

A portion of this research at Oak Ridge National Laboratory's Spallation Neutron Source was sponsored by the U.S. Department of Energy, Office of Basic Energy Sciences.

Ivelisse Cabrera's review and comments regarding the manuscript are greatly appreciated.

Instrumental resolution convolutions performed by Jiao Lin are acknowledged with gratitude. Matt Stone also assisted with many helpful discussions.

References

[1] L. Van Hove, Phys. Rev. 95 (1954) 249–262.

[2] D. Parks, M. Nelkin, J. Beyster, M. Wikner, Slow Neutron Scattering and Thermalization, W. A. Benjamen, Inc., New York, New York, 1970.

[3] P. A. Egelstaff, P. Schofield, Nucl. Sci. and Eng. 12 (2) (1962) 260–270.

[4] R. E. MacFarlane, Springer US, 2010, pp. 189–277.

[5] T. Goorley, et al., Initial mcnp6 release overview, Nuclear Technology 180 (3) (2012) 298–315.

[6] J. U. Koppel, D. H. Houston, Reference manual for thermal neutron scattering data, Report ENDF-269 (1969).

[7] D. Brown, et al., Nuclear Data Sheets 148 (2018) 1 – 142, special Issue on Nuclear Reaction Data.

[8] C. Lavelle, C.-Y. Liu, M. Stone, Nucl. Inst. Meth. A 711 (2013) 166 – 179.

[9] E. Farhi, G. Ferran, W. Haeck, E. Pellegrini, Y. Calzavara, J. Nucl. Sci. and Tech. 52 (6) (2015) 844–856.

[10] K. Ramić, et al., Annals of Nuclear Energy 120 (2018) 778–787.

[11] ND 2019: International conference on nuclear data for science and technology, beijing, china, may 19-24, 2019, EPJ Web of Conferences 239 (2009).

[12] J. I. Márquez Damián, private communication (2020).

[13] K. Ramić, et al., Annals of Nuclear Energy 133 (2019) 425–430.

[14] R. MacFarlane, A. Kahler, Nuclear Data Sheets 111 (12) (2010) 2739 – 2890.

[15] R. E. MacFarlane, Neutron Slowing Down and Thermalization Handbook of Nuclear Engineering, Springer US, 2010, pp. 189–277.

[16] D. L. Abernathy, M. B. Stone, M. J. Loguillo, M. S. Lucas, O. Delaire, X. Tang, J. Y. Y. Lin, B. Fultz, Rev. Sci. Inst. 83 (1) (2012) 015114.

[17] J. Dawidowski, G. Cuello, M. Koza, J. Blostein, G. Aurelio, A. F. Guillermet, P. Donato, Nucl. Inst. Meth. B 195 (2002) 389–399.

[18] J. Conlin, et al., Continuous-s(α,β) capability in mcnp, Report LA-UR-00155 (2012).

[19] J. Parsons, D. K. Conlin, et al., Release of continuous representation for S(a,b) ACE data, Report LA-UR-12-00800 (2012).

[20] National Nuclear Data Center (NNDC) Cross Section Evaluation Working Group (CSEWG).

[21] J. Lin, M. Stone, private communication (Feb. 2021).

[22] G. D. Barrera, S. F. Parker, A. J. Ramirez-Cuesta, P. C. H. Mitchell, Macromolecules 39 (7) (2006) 2683–2690.

[23] Downloaded from http://www.njoy21.io/.

[24] A. I. Hawari, A. Petersen, Y. Zhu, D. P. Heinrichs, M. L. Zerkle, Transactions of the American Nuclear Society 115 (1) (2016) 689–691.

C. M. Lavelle: Methodology, Software, Formal Analysis, Visualization, Writing- original draft. K. K. H. Leung: Methodology, Investigation, Writing- Reviewing and Editing. T. Ito: Conceptualization, Methodology, Investigation, Project administration.

Declaration of interests

☒ The authors declare that they have no known competing financial interests or personal relationships that could have appeared to influence the work reported in this paper.

☐The authors declare the following financial interests/personal relationships which may be considered as potential competing interests: